RSC Advances

PAPER

View Article Online
View Journal | View Issue

Cite this: *RSC Adv.*, 2017, **7**, 3752

High-rate-capability asymmetric supercapacitor device based on lily-like Co_3O_4 nanostructures assembled using nanowires†

Yanjie Wang,[a] Shaobo Huang,[a] Yin Lu,[a] Shizhong Cui,[a] Weihua Chen*[b] and Liwei Mi*[a]

Following the growing demand for high-efficient energy storage systems, high-current-density supercapacitor devices are needed; however, their development is still a challenge. An electrode material with high electronic conductivity and abundant ion channels is an important area of research. Herein, hierarchical lily-like Co_3O_4 nanostructures constituted using nanowires with a large *L*/*D* ratio on Ni foam were *in situ* synthesized using a simple solvent-thermal method and subsequent sintering treatment. The as-prepared Co_3O_4 precursor was composed of nanowires with a ~50 nm average diameter and ~70 *L*/*D* ratio. The product morphology was well maintained after thermal treatment, and the product was transformed to cubic Co_3O_4 during this process. Co_3O_4/Ni exhibited excellent rate capability and cycling performance, which showed a specific capacitance of 1600 F g^{-1} even at a relatively high 10 A g^{-1} current density that barely declined after 5000 cycles. Furthermore, the assembled asymmetric supercapacitor device using the as-prepared Co_3O_4/Ni and activated carbon showed a high specific capacitance at a high current density (108.1 F g^{-1} at a current density of 0.5 A g^{-1}, 96.4 F g^{-1} at 10 A g^{-1} and 77.9 F g^{-1} even at 50 A g^{-1}) and displayed a long-term cycling stability performance (10 000 cycles) with a high energy density (34 W h kg^{-1}) at a high power density of 1963 W kg^{-1}. The superior performance of lily-like Co_3O_4 nanostructures on Ni foam is proposed to be attributed to benign electronic conductivity and the presence of abundant ion transport channels. Therefore, these experimental results suggest the potential application of cobalt-based oxides in a high-current-density electrochemical system.

Received 26th November 2016
Accepted 21st December 2016

DOI: 10.1039/c6ra27356d

www.rsc.org/advances

Introduction

Following the over-exploitation of fossil fuels with rapid economic development, energy crisis is becoming increasingly serious.[1] Therefore, clean sustainable energy or high-efficiency energy storage/conversion system is urgent to be developed in order to improve the energy utilization efficiency.[2–4] For example, following the pressing demand for mobile devices and electro mobiles with fast-charge and high energy storage properties, there is an urgency to develop a high-efficiency electrochemical storage device.[1,2,5] To date, lithium/sodium ion batteries, lithium–sulfur batteries, supercapacitors and so on, have received considerable attention.[6–21] Among them, supercapacitors possess unique advantages of fast charge/discharge, environment friendliness and a long lifetime.[5] Significant efforts have been devoted in developing high-energy-density, long cycling life supercapacitors.[22] Compared with electric double-layer capacitors, pseudocapacitors exhibit higher specific capacitance due to fast redox reactions on the surface of electrode materials.[22,23] However, the cycling life and rate performance of the pseudocapacitors is unsatisfactory.[22] To meet the urgent demand in high-efficiency electrical equipment, improving the long-term cycling life and excellent rate performance of supercapacitors is imperative. The electrode material is the key part of a supercapacitor device and has a decisive effect on the supercapacitor performance.[5] Therefore, much effort has been made on the design and exploitation of electrode materials with higher specific capacitance and long cycling life.[2,22–24] However, a high-current-density supercapacitor device is needed to be developed, which is still a challenge.[22]

The ideal electrode material for a supercapacitor probably possesses the properties of high electronic conductivity and abundant ion channels.[1,2,5,22–24] In recent years, the research in electrode materials for supercapacitors has mainly concentrated on carbon,[25,26] conducting polymers,[27] metal oxides,[28–35] metal sulfides,[36–38] and so on.[2] Among them, metal oxides, for

[a]*Center for Advanced Materials Research, Zhongyuan University of Technology, Zhengzhou, Henan 450007, China. E-mail: mlwzzu@163.com*

[b]*College of Chemistry and Molecular Engineering, Zhengzhou University, Zhengzhou, Henan, 450001, China. E-mail: chenweih@zzu.edu.cn*

† Electronic supplementary information (ESI) available: The FT-IR spectrum (Fig. S1), EDS result (Fig. S2) of Co-precursor and the pictures of LED (Fig. S3) powered by two supercapacitors in series at different times. See DOI: 10.1039/c6ra27356d

example Co_3O_4,[29] NiO,[30] MnO_2,[31] are considered as important candidate electrode materials in supercapacitors due to their high specific capacitance. However, inferior electronic conductivity of metal oxides greatly hinders electron transport and thus weakens the rate and cycling performance of supercapacitors. Therefore, compositing the conductive material (*e.g.* metal or carbon materials) with these electrode materials is probably an effective approach to overcome this problem.[24,39,40] Nickel foam possesses fine electronic conductivity and ductility, which can be considered as an ideal supporter in electrochemical power sources.[41]

The size and morphology of electrode materials greatly determine the exposed active surface, which show a significant effect on the electrochemical behavior of the supercapacitor device.[2] A large specific surface area can accelerate surface redox reactions and enhance the contact between the active material and electrolyte. By decreasing the size, the electrode materials can expose more active surface, thus enhancing the specific surface area and shortening the ion channel, to finally improve the electrochemical performance. The morphology of electrode materials is also an important factor that influences electrochemical behavior. Due to the unique structure and high number of exposed active sites, one-dimensional nanostructures (*e.g.* nanowires, nanorods, nanotubes) have been devoted large attention in catalysis and energy storage/conversion fields. For example, carbon nanotubes, Co_3O_4 nanorods, MnO_2 nanotubes, and so on have been applied in the electrode material of lithium ion batteries or supercapacitors.[42–47] As mentioned previously, electrode materials with high specific capacitance and long term cycling for high performance supercapacitors should be equipped with high specific area and excellent electronic conductivity. Therefore, constructing the composite nanostructure of one-dimensional metal oxide with a conductive metal support is probably an effective approach to design an advanced supercapacitor device. For example, one-dimensional Co_3O_4 nanostructures showed preferable electrochemical properties in previous studies.[48–52] To date, large attention has been drawn towards using different methods for the synthesis of one dimensional Co_3O_4 nanostructures with excellent electrochemical properties (*e.g.* hydro-thermal method).[53,54] However, high-current-density supercapacitor devices based on cobalt-based materials are rarely reported and remain a current challenge.

In this study, hierarchical lily-like Co_3O_4 microflowers on Ni foam, which are assembled using nanowires, were fabricated *via* a simple solvent-thermal method and subsequent sintering treatment. Systematic characterizations were conducted to understand the formation mechanism and electrochemical behavior of the as-prepared product. The electrochemical performance (specific capacitance, long cycling life, energy density, power density) were evaluated in three-electrode and two-electrode systems assembled using the as-prepared Co_3O_4 on Ni foam and activated carbon (Co_3O_4/Ni//AC). In addition, practical application was evaluated through choosing the commercial light-emitting diodes (LEDs) as a load model.

Experimental

Synthesis of Co_3O_4 nanostructures

All chemical reagents were of analytical grade and used without further purification. $Co(NO_3)_3 \cdot 6H_2O$ (0.5 mmol) and urea ($CO(NH_2)_2$) (10 mmol) were dissolved in a mixed solvent (4 mL ethanol, 16 mL H_2O). After stirring on a magnetic stirring apparatus for 20 min, Ni foam was put into the abovementioned mixed solution. Then, the mixed suspension was transferred into a Teflon-lined stainless steel autoclave and heated at 150 °C for 15 h. The products (Co-precursor) were washed with deionized water and ethanol and further dried at 80 °C overnight. Finally, Co-precursor was heated at 350 °C for 2 h in an Ar atmosphere to obtain a Co_3O_4 sample on Ni foam. In addition, for comparison, Co_3O_4 powder was obtained from a similar method to the abovementioned method for Co_3O_4 sample on Ni foam except for the absence of Ni foam. The mass loading of Co_3O_4 on Ni foam was calculated through a difference method. The mass loading of Co_3O_4 for further measurement is about 2 mg ($\sim$2 mg cm^{-2}).

Instrument and characterization

To realize the physical and chemical properties of the Co_3O_4 sample, some characterizations were carried out. The morphology of product was checked with a Zeiss Merlin Compact field emission scanning electron microscope (FESEM) equipped with an energy-dispersive X-ray spectroscopy (EDX) system. The microstructure and composition of the as-prepared Co_3O_4 sample were detected *via* transmission electron microscopy (TEM, JEOL, JEM-2100) and high-resolution TEM (HR-TEM, JEOL JEM-2010F). We examined the phase *via* X-ray diffraction (XRD) on a Bruker D8 Advance X-ray powder diffractometer using Cu-Kα irradiation at a scan rate of 4° min^{-1}.

Electrochemical properties measurement

All the electrochemical measurements were carried out using a galvanostatic charge/discharge tester (CT2001A) and electrochemical workstation (CHI 660E) in both standard three-electrode mode and two-electrode mode. For the two-electrode mode, the working electrode was the as-prepared Co_3O_4 product on Ni foam, and the counter electrode was activated carbon (AC) on Ni foam (in which the active carbon, acetylene black, polyvinylidene fluoride (PVDF) with an 8 : 1 : 1 mass ratio). The working electrode and counter electrode can be separated with a piece of nonwoven separator in 1 M KOH solution. For the three-electrode mode, the reference electrode was a Hg/HgO electrode, and the other conditions (for example, working electrode and electrolyte) were similar to the two-electrode mode. Furthermore, the specific capacitance (C), energy density (E) and power density (P) could be calculated from the charge/discharge curve as follows:

$$C = I\Delta t/m\Delta V \text{ (F g}^{-1}\text{)} \quad (1)$$

where I represents constant discharge current, Δt represents discharge time, m represents the mass of active material, and ΔV represents width of the potential widow.

$$E = 1/2(C\Delta V^2) \quad (2)$$

$$P = E/\Delta t \quad (3)$$

The electrochemical impedance spectroscopy (EIS) data were recorded using a CHI660E electrochemical workstation (Chenhua, Shanghai, China) in the 0.01 Hz and 100 kHz frequency range. In addition, the commercial red light-emitting diodes (LEDs) as a load model were lightened by connecting two Co_3O_4/Ni//AC supercapacitor devices in series, which were charged at a current density of 5 A g^{-1}.

Results and discussion

Synthesis and characterization

The Co_3O_4 product was fabricated through sintering treatment of the as-prepared precursor (Co-precursor), which was prepared *via* a simple solvent-thermal method. Fig. 1 shows the SEM images of the as-prepared Co-precursor and Co_3O_4 product under different magnifications. Shown from Fig. 1a, the obtained Co-precursor has lily-like nanostructures composed of one-dimensional nanowires. The petal was assembled using nanowires with different length/diameter (L/D) ratios, and some nanowires even would be curved due to the large L/D ratio. After calculation, the L/D ratio of the petal was about ~70. The pistil was assembled using shorter nanorods. From the high-resolution SEM image in Fig. 1b, the diameter of nanowire or nanorod was about ~50 nm. After thermal treatment, the morphology of product was well maintained from the precursor, except that the nanowire changed from smooth to rough. The one-dimensional nanowires could be observed to consist of nanoparticles based on high-resolution SEM imaging of the Co_3O_4 product, which is shown in Fig. 1d. The rough one-dimensional nanowires, which appeared like a necklace, probably possessed a high exposure to surface and sites, which facilitated the electron transfer.

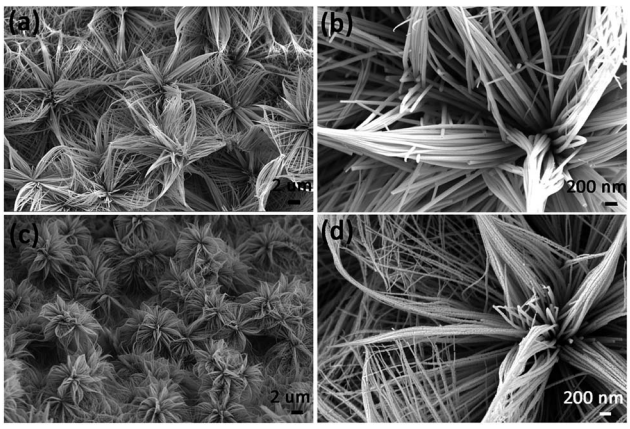

Fig. 1 The SEM images of as-prepared Co-precursor ((a) and (b)) and Co_3O_4 product ((c) and (d)).

XRD characterization can give us the phase information of a sample. Fig. 2a shows XRD spectra of the as-prepared precursor and Co_3O_4 product. The peak of Ni foam is evident from the XRD spectra of the as-prepared precursor and Co_3O_4. However, other XRD peaks of as-prepared precursor cannot be indexed, which is probably due to the precursor being a complex. We further measured the FT-IR spectrum and the energy dispersive spectrum (EDS) to understand the composition of the as-prepared precursor, and the results are shown in Fig. S1 and S2.† Combining the analysis of FT-IR spectrum and EDS spectrum, the precursor was proposed to be a Co complex containing the Co, O, C elements, at least due to the coordination role between cobalt ion and organic components. After thermal treatment, apart from the signal of Ni foam, the peak (37°) of the XRD spectrum of the Co_3O_4 product was well indexed with the cubic Co_3O_4 (JCPDS 00-009-0418) from the inset spectrum, indicating the purity of the Co_3O_4 sample. In addition, the existence of the cobalt element was directly verified by the EDS spectrum, as shown in Fig. 2b. For further understanding the microstructure of the as-prepared product, TEM analysis was also conducted. From the TEM image of Co_3O_4 microstructures in Fig. 2c, the diameter of nanowire was found to be about ~50 nm, and they were composed of nanoparticles. The lattice distance calculated from HRTEM image in Fig. 2d is 4.65 Å was in good accordance with the standard lattice distance {111} of cubic Co_3O_4. The abovementioned TEM analysis was consistent with the XRD results. Therefore, considering the XRD results and TEM analysis, the cubic Co_3O_4 with high quality was successfully acquired.

For further understanding the formation mechanism of lily-like Co_3O_4 nanostructures, the effect of dosage of the cobalt salt on product was investigated and the corresponding SEM images are shown in Fig. 3. Shown in Fig. 3, when the dosage of cobalt salt was low (1 and 2 mmol), the morphology of product was shorter nanorods. As the cobalt salt dosage was increased, the nanorods gradually elongated. When the dosage of cobalt salt was increased to 4 mmol, the morphology of the product was nanowires. When the dosage of cobalt salt was increased to 5 mmol, the L/D ratio increased and even become curved. Three-dimensional hierarchical nanostructures gradually formed on further addition of the cobalt salt. The proposed formation mechanism of lily-like Co_3O_4 nanostructures is shown in Scheme 1. In the reaction process, the Co ions can be absorbed on the surface of Ni foam and can be transformed to one-dimensional complex Co compound nanorods in the presence of urea. Following the reaction, the nanorods enlarged and assembled into three-dimensional lily-like Co_3O_4 nanostructures.

Electrochemical performance

The electrochemical properties of the as-prepared Co_3O_4/Ni product, as a supercapacitor electrode material, were evaluated in three- and two-electrode systems. Fig. 4 demonstrates the cyclic voltammetry (CV) curves tested at different scan rates and charge–discharge performance of as-prepared product in the three-electrode system. From the cyclic voltammetry (CV) curves of Co_3O_4/Ni at different scan rates with 1 M KOH electrolyte at

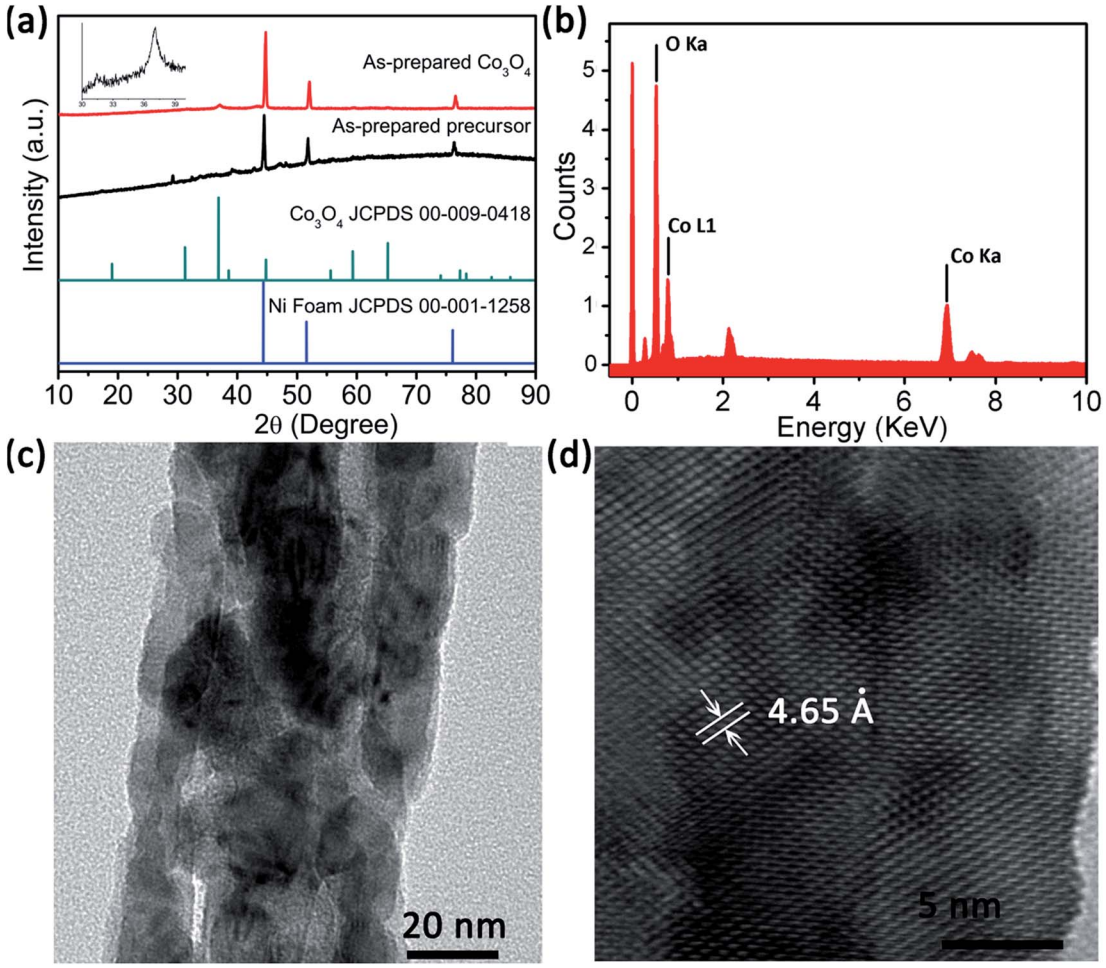

Fig. 2 (a) The XRD spectra of the as-prepared Co-precursor and Co_3O_4 products, (b) EDS spectrum of the as-prepared Co_3O_4 products, (c) TEM image of the as-prepared Co_3O_4 product, (d) HRTEM spectrum of the as-prepared Co_3O_4 products.

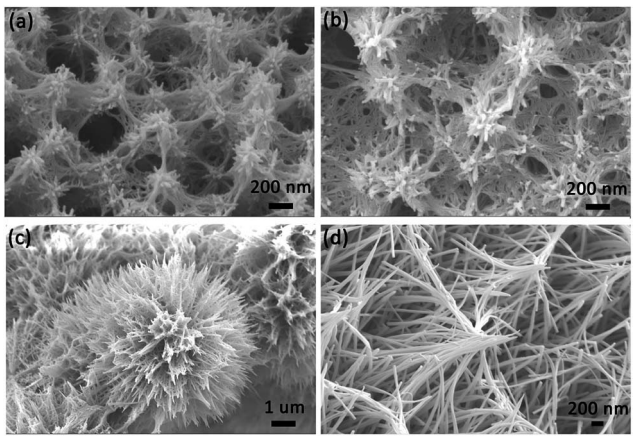

Fig. 3 SEM images of the as-prepared Co-precursor at different concentrations of cobalt salt. (a) 1 mmol, (b) 2 mmol, (c) 3 mmol, (d) 4 mmol.

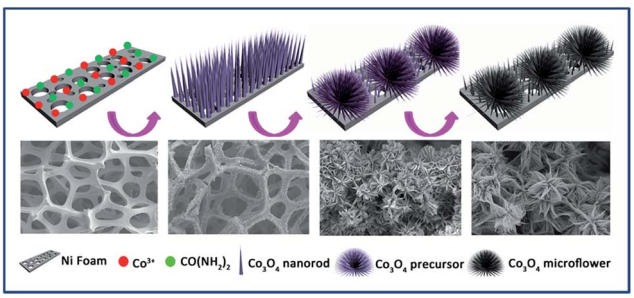

Scheme 1 The proposed formation mechanism of lily-like Co_3O_4 nanostructures.

a potential sweep window 0–0.6 V (Fig. 4a), redox peaks can be clearly observed, indicating pseudocapacitive behavior of cobalt oxides due to the redox reaction between Co^{2+} and Co^{3+}. Fig. 4b exhibits CV curves of sample after 2000 cycles, which are similar to the original CV curves, indicating the cyclic stability of as-prepared Co_3O_4 electrode. Fig. 4c displays the charge–discharge curves and Fig. 4d shows the rate capability of as-prepared Co_3O_4/Ni. The discharge time at the current densities of 0.5, 1, 2, 5, 10 A g^{-1} is 1847, 905, 445, 177, 88 s, respectively. The corresponding specific capacitance of Co_3O_4/Ni was 1679, 1645, 1618, 1609, and 1600 F g^{-1} at the current densities

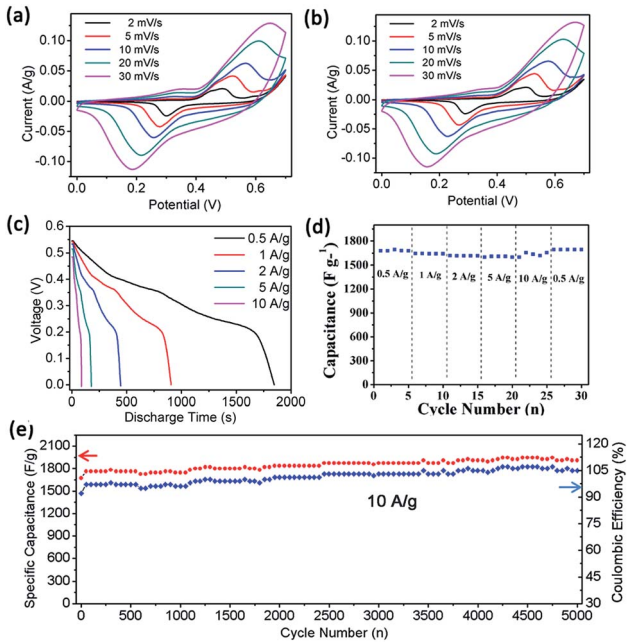

Fig. 4 Electrochemical properties of the as-prepared Co_3O_4 product in a three-electrode system. (a) Cyclic voltammetry (CV) curves, (b) CV curves after 2000 cycles, (c) discharge curves at different current density, (d) rate capability, and (e) specific capacitance and columbic efficiency during cycling.

of 0.5, 1, 2, 5 and 10 A g^{-1}, respectively, indicating excellent discharge performance at a high current density. This excellent rate capability demonstrated superior discharge performance at high current density, which has potential application in commercial supercapacitors. In addition, the specific capacitance barely declined after 5000 cycles at a current density of 10 A g^{-1} (Fig. 4e). Compared with those in previous studies (Table 1), the specific capacitance and cycling performance at high current density is notably improved.[48–52,55–57]

The asymmetric supercapacitor device was further assembled with the as-prepared Co_3O_4/Ni and active carbon (Co_3O_4/Ni//AC). The electrochemical performance was evaluated and the results are shown in Fig. 5. The cyclic voltammetric (CV) curves of Fig. 5a were tested at a scan rate of 2–100 mV s^{-1} with 1 M KOH electrolyte at a potential sweep window of 0–1.6 V. The shape of curves is deviated from the ideal rectangular voltammogram due to the pseudocapacitive behavior of cobalt oxides. Based on that, pure Ni foam has little contribution to the capacitance, and the pseudocapacitive behavior is attributed to the as-prepared cobalt oxides. Fig. 5b and c give the discharge curves of Co_3O_4/Ni//AC device. When the current density was 0.5 A g^{-1}, the discharge time of Co_3O_4/Ni//AC device was high, 1477 s (the specific capacitance was 108.1 F g^{-1}). When the current density increased to 10 A g^{-1}, the discharge time was 76 s (the specific capacitance was 96.4 F g^{-1}). Fig. 5d exhibits the rate capacity of the Co_3O_4/Ni//AC device. When the current density was increased to 20 A g^{-1} and even 50 A g^{-1}, the specific capacitances were still maintained at 86 F g^{-1} and 78 F g^{-1}, indicating the potential application in fast charge–discharge devices. Fig. 5e exhibits the cycling performance and coulombic efficiency of Co_3O_4/Ni//AC device and Co_3O_4 powder//AC device. Compared with Co_3O_4 powder, Co_3O_4/Ni//AC device possessed higher cycling capacity and coulombic efficiency. As shown in Fig. 5e, the specific capacitance of the Co_3O_4/Ni//AC device was faultlessly maintained at a high current density of 10 A g^{-1} after 10 000 cycles. It is proposed that the Ni substrate and binder-free equipment method increased the electron conductivity of Co_3O_4.

We further conducted electrochemical impedance spectroscopy (EIS) measurement and the result is shown in Fig. 6a, where the impedance of Co_3O_4/Ni decreased evidently. In addition, the relationship between energy density (E) and power density (P) is represented in Fig. 6b. As is known, Co_3O_4/Ni//AC supercapacitor device density of 1973 W kg^{-1} also can be as

Table 1 The electrochemical supercapacitor performance in previous studies[a]

References	Material	C^t (F g^{-1})	E^d (W h kg^{-1})
Ref. 48	Co_3O_4@MnO_2	560 (0.2 A g^{-1})	17.7 (158 W kg^{-1})
Ref. 49	Co_3O_4/rGO/CNT	790 (1 A g^{-1})	19.6 (7250 W kg^{-1})
Ref. 50	Co_3O_4/graphene	494.2 (7.2 A g^{-1})	—
Ref. 56	Co_3O_4	378 (1 A g^{-1})	—
Ref. 57	3D Co_3O_4-rGO	660 (0.5 A g^{-1})	40.65 (340 W kg^{-1})
This work	Co_3O_4/Ni foam	1600 (10 A g^{-1})	34 (1963 W kg^{-1})

[a] Note: C^t represents the specific capacitance in a three-electrode mode, E^d represents the energy density in a two-electrode mode.

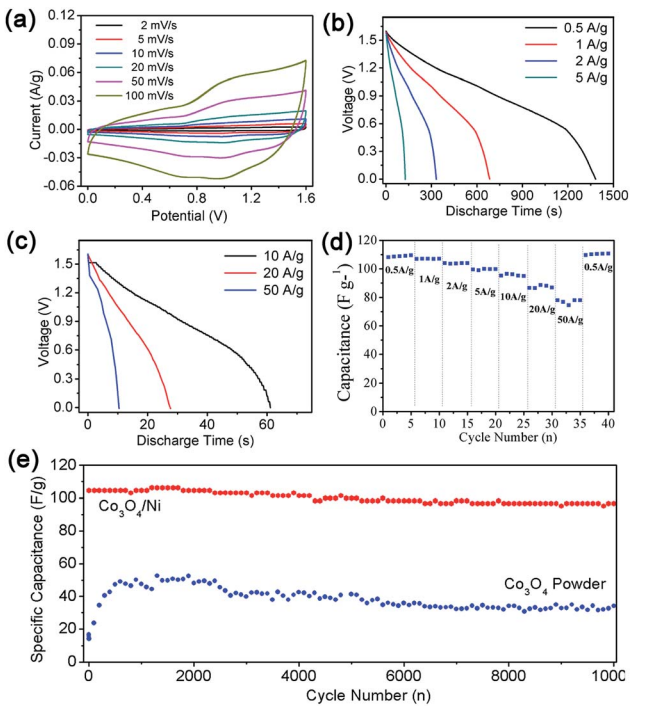

Fig. 5 The electrochemical properties of as-prepared Co_3O_4 product in a two-electrode system. (a) Cyclic voltammetry (CV) curves, (b) and (c) the discharge curves at different current density, (d) the rate capability of Co_3O_4/Ni//AC device, and (e) the specific capacitance of Co_3O_4/Ni//AC and Co_3O_4 powder//AC devices.

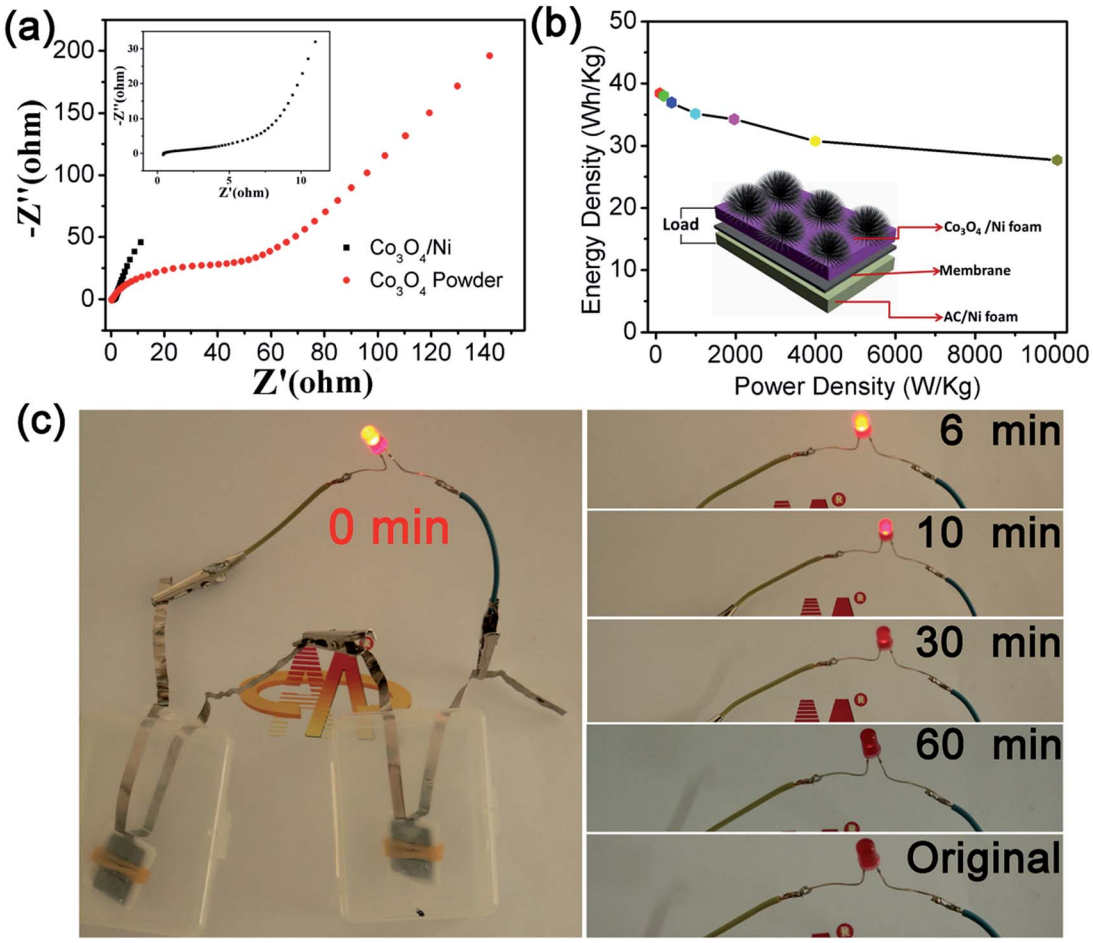

Fig. 6 (a) The electrochemical impedance spectra of as-prepared Co_3O_4/Ni and Co_3O_4 powder. (b) The energy density and power density of Co_3O_4/Ni//AC asymmetric supercapacitor. (c) The brightness of LED lightened by two supercapacitor devices in series.

high as 34 W h kg^{-1}, which displays a maximum energy density of 38 W h kg^{-1} at a power density of 100 W kg^{-1}. Importantly, the energy density at a power confirmed the excellent rate capability of the Co_3O_4/Ni//AC supercapacitor device. Importantly, the power density could be as high as 10 060 W kg^{-1}. These results demonstrated excellent electrochemical energy storage performance of Co_3O_4/Ni electrode material and indicated commercial high-current supercapacitor device potential due to the superior rate capability. Therefore, this outstanding performance of the as-prepared binder-free Co_3O_4 electrode material is proposed to be attributed to good electronic conductivity resulting from the Ni substrate and abundant ion channels resulting from the one-dimensional structure. Moreover, practical application was evaluated through choosing the commercial light-emitting diodes (LEDs) as a load model by connecting two Co_3O_4/Ni//AC supercapacitor devices in series, and the results are shown in Fig. 6c. After a successful series connection, the LED was lit (0 min) compared with the unconnected state (original), and then the brightness gradually descended following the connection (6 min, 10 min, 30 min). After 60 min, the LED brightness was weak but still visible, and this state could be maintained for another 90 min. The entire continuous brightness change of LED is presented in Fig. S3.†

Conclusion

In conclusion, using a simple solvent-thermal method and subsequent sintering treatment, lily-like Co_3O_4 nanostructures on Ni foam were successfully prepared. XRD analysis indicated high purity of the as-prepared Co_3O_4 product. SEM images showed that the as-prepared Co_3O_4 nanostructures were composed of nanowires with large L/D ratio (~70) and an average diameter of ~50 nm. The specific capacitance of the as-prepared Co_3O_4 nanostructures at a high current densities of 5 A g^{-1}, and 10 A g^{-1} were 1609 F g^{-1} and 1600 F g^{-1}, respectively, exhibiting excellent rate performance. The specific capacitance was perfectly maintained after 5000 cycles even at a high current density of 10 A g^{-1} after 5000 cycles. Furthermore, the assembled asymmetric supercapacitor device using the as-prepared Co_3O_4/Ni and activated carbon exhibited a high specific capacitance (108.1 F g^{-1} and 96.4 F g^{-1} at current densities of 0.5 A g^{-1} and 10 A g^{-1}, respectively) and displayed a long-term cycling performance with a high energy density (34 W h kg^{-1}) at a power density of 1963 W kg^{-1}. Importantly, the maximum power density could be as high as 10 060 W kg^{-1}. Moreover, the Co_3O_4/Ni//AC device presented an excellent performance over a Co_3O_4 powder device due to the benign electronic conductivity

resulting from the Ni substrate and abundant ion transport channels resulting from the one-dimensional structure. These results demonstrated the excellent electrochemical energy storage performance of the Co_3O_4/Ni electrode material and indicated it to be a commercial high-current supercapacitor device due to its superior rate capability.

Acknowledgements

Thanks a lot for the support from the Natural Science Foundation of China (No. 21443003 & U1407103), Henan Province (No. 15HASTIT003), Innovation Scientists and Technicians Troop Construction Projects of Henan Province and Zhengzhou University (No. 1421316035).

Notes and references

1 W. Y. Hernández, O. H. Laguna, M. A. Centeno, A. S. AricÒ, P. Bruce, B. Scrosati, J. M. Tarascon and W. V. Schalkwijk, *Nat. Mater.*, 2005, **4**, 366–377.
2 Y. G. Guo, J. S. Hu and L. J. Wan, *Adv. Mater.*, 2008, **20**, 2878–2887.
3 Y. Zhao, X. Jia, G. Chen, L. Shang, G. I. N. Waterhouse, L. Z. Wu, C. H. Tung, D. O'Hare and T. Zhang, *J. Am. Chem. Soc.*, 2016, **138**, 6517–6524.
4 Y. Zhao, X. Jia, G. I. N. Waterhouse, L. Z. Wu, C. H. Tung, D. O'Hare and T. Zhang, *Adv. Energy Mater.*, 2016, **6**, 1501974.
5 P. Simon and Y. Gogotsi, *Nat. Mater.*, 2008, **7**, 845–854.
6 J. M. Tarascon and M. Armand, *Nature*, 2001, **414**, 359–367.
7 M. A. Rahman, G. Song, A. I. Bhatt, Y. C. Wong and C. Wen, *Adv. Funct. Mater.*, 2015, **26**, 647–678.
8 Y. Yang, G. Zheng and Y. Cui, *Chem. Soc. Rev.*, 2013, **42**, 3018–3032.
9 X. Ji, K. T. Lee and L. F. Nazar, *Nat. Mater.*, 2009, **8**, 500–506.
10 X. Lu, T. Zhai, X. Zhang, Y. Shen, L. Yuan, B. Hu, L. Gong, J. Chen, Y. Gao, J. Zhou, Y. Tong and Z. L. Wang, *Adv. Mater.*, 2012, **24**, 938–944.
11 Y. Zhang, X. Rui, Y. Tang, Y. Liu, J. Wei, S. Chen, W. R. Leow, W. Li, Y. Liu, J. Deng, B. Ma, Y. Yan and X. Chen, *Adv. Energy Mater.*, 2016, **6**, 1502409.
12 Z. Niu, W. Zhou, X. Chen, J. Chen and S. Xie, *Adv. Mater.*, 2015, **27**, 6002–6008.
13 Z. Niu, L. Liu, L. Zhang, W. Zhou, X. Chen and S. Xie, *Adv. Energy Mater.*, 2015, **5**, 1500677.
14 H. Xu, X. Hu, Y. Sun, W. Luo, C. Chen, Y. Liu and Y. Huang, *Nano Energy*, 2014, **10**, 163–171.
15 X. Xu, H. Hu, H. Yang, Y. Sun, C. Hu and Y. Huang, *Adv. Energy Mater.*, 2015, **5**, 1401882.
16 Y. M. Chen, L. Yu and X. W. Lou, *Angew. Chem., Int. Ed.*, 2016, **55**, 5990–5993.
17 H. Hu, B. Y. Guan, B. Y. Xia and X. W. Lou, *J. Am. Chem. Soc.*, 2015, **137**, 5590–5595.
18 G. X. Gao, H. B. Wu, S. J. Ding, L. M. Liu and X. W. Lou, *Small*, 2015, **11**, 804–808.
19 F. F. Cao, M. T. Zhao, Y. F. Yu, B. Chen, Y. Huang, J. Yang, X. H. Cao, Q. P. Lu, X. Zhang, Z. C. Zhang, C. L. Tan and H. Zhang, *J. Am. Chem. Soc.*, 2016, **138**, 6924–6927.
20 G. A. Sun, J. Q. Liu, X. Zhang, X. W. Wang, H. Li and Y. Yu, *Angew. Chem., Int. Ed.*, 2014, **53**, 12576–12580.
21 N. Choudhary, C. Li, H. S. Chung, J. Moore, J. Thomas and Y. Jung, *ACS Nano*, 2016, **10**, 10726–10735.
22 G. Wang, L. Zhang and J. Zhang, *Chem. Soc. Rev.*, 2012, **41**, 797–828.
23 M. Yu, Y. Zeng, Y. Han, X. Cheng, W. Zhao, C. Liang, Y. Tong, H. Tang and X. Lu, *Adv. Funct. Mater.*, 2015, **25**, 3534–3540.
24 J. Wu, C. Ouyang, S. Dou and S. Wang, *Nanotechnology*, 2015, **26**, 325401.
25 Y. Wang, H. Wei, Y. Lu, S. Wei, E. Wujcik and Z. Guo, *Nanomaterials*, 2015, **5**, 755–777.
26 Y. Song, Z. Li, K. Guo and T. Shao, *Nanoscale*, 2016, **8**, 15671–15680.
27 Y. Shi, L. Peng, Y. Ding and G. Yu, *Chem. Soc. Rev.*, 2015, **44**, 6684–6696.
28 Q. Liao, N. Li, S. Jin, G. Yang and C. Wang, *ACS Nano*, 2015, **9**, 5310–5317.
29 L. Xie, F. Su, L. Xie, X. Li, Z. Liu, Q. Kong, X. Guo, Y. Zhang, L. Wan, K. Li, C. Lv and C. Chen, *ChemPubSoc*, 2015, **8**, 2917–2926.
30 X. Dong, Z. Guo, Y. Song, M. Hou, J. Wang, Y. Wang and Y. Xia, *Adv. Funct. Mater.*, 2014, **24**, 3405–3412.
31 L. F. Chen, Z. H. Huang, H. W. Liang, Q. F. Guan and S. H. Yu, *Adv. Mater.*, 2013, **25**, 4746–4752.
32 W. Wen, J. M. Wu, Y. Z. Jiang, J. Q. Bai and L. L. Lai, *J. Mater. Chem. A*, 2016, **4**, 10593–10600.
33 W. Wen and J. M. Wu, *ACS Appl. Mater. Interfaces*, 2011, **3**, 4112–4119.
34 W. Wen, J. M. Wu and M. H. Cao, *J. Mater. Chem. A*, 2013, **1**, 3881–3885.
35 W. Wen, J. M. Wu and M. H. Cao, *Nano Energy*, 2013, **2**, 1383–1390.
36 L. Mi, W. Wei, S. Huang, S. Cui, W. Zhang, H. Hou and W. Chen, *J. Mater. Chem. A*, 2015, **3**, 20873–20982.
37 Y. Gao, L. Mi, W. Wei, S. Cui, Z. Zheng, H. Hou and W. Chen, *ACS Appl. Mater. Interfaces*, 2015, **7**, 4311–4319.
38 W. Wei, L. Mi, S. Cui, B. Wang and W. Chen, *ACS Sustainable Chem. Eng.*, 2015, **3**, 2777–2785.
39 J. Zhu, J. Jiang, Z. Sun, J. Luo, Z. Fan, X. Huang, H. Zhang and T. Yu, *Small*, 2014, **10**, 2937–2945.
40 D. Gu, D. W. Li, F. Wang, H. Bongard, B. Spliethoff, W. Schmidt, C. Weidenthaler, Y. Xia, D. Zhao and F. Schuth, *Angew. Chem., Int. Ed.*, 2015, **54**, 7060–7064.
41 C. Yuan, J. Li, L. Hou, L. Yang, L. Shen and X. Zhang, *Electrochim. Acta*, 2012, **78**, 532–538.
42 H. Xia, D. Zhu, Z. Luo, Y. Yu, X. Shi, G. Yuan and J. Xie, *Sci. Rep.*, 2013, **3**, 2978–2985.
43 Z. Su, C. Yang, B. Xie, Z. Lin, Z. Zhang, J. Liu, B. Li, F. Kang and C. P. Wong, *Energy Environ. Sci.*, 2014, **7**, 2652–2659.
44 P. Vialat, C. Mousty, C. Taviot-Gueho, G. Renaudin, H. Martinez, J. C. Dupin, E. Elkaim and F. Leroux, *Adv. Funct. Mater.*, 2014, **24**, 4831–4842.
45 Y. Hu, C. Guan, G. Feng, Q. Ke, X. Huang and J. Wang, *Adv. Funct. Mater.*, 2015, **25**, 7291–7299.
46 Z. Yu, B. Duong, D. Abbitt and J. Thomas, *Adv. Mater.*, 2013, **25**, 3302–3306.

47 Y. Kim, J. H. Lee, S. Cho, Y. Kwon, I. In, J. Lee, N. H. You, E. Reichmanis, H. Ko, K. T. Lee, H. K. Kwon, D. H. Ko, H. Yang and B. Park, *ACS Nano*, 2014, **8**, 6701–6712.
48 M. Huang, Y. Zhang, F. Li, L. Zhang, Z. Wen and Q. Liu, *J. Power Sources*, 2014, **252**, 98–106.
49 N. Kumar, C. W. Huang, P. J. Yen, W. W. Wu, K. H. Wei and T. Y. Tseng, *RSC Adv.*, 2016, **6**, 60578–60586.
50 Y. Li, S. Zhang, Q. Chen and J. Jiang, *Int. J. Electrochem. Sci.*, 2015, **10**, 6199–6212.
51 A. K. Singh, D. Sarkar, K. Karmarkar, K. Mandal and G. G. Khan, *ACS Appl. Mater. Interfaces*, 2016, **8**, 20786–20792.
52 M. Kim, J. Choi, H. Oh and J. Kim, *Phys. Chem. Chem. Phys.*, 2016, **18**, 19696–19704.
53 X. Yang, H. Li, A. Y. Lu, S. Min, Z. Idriss, M. N. Hedhili, K. W. Huang, H. Ideiss and L. J. Li, *Nano Energy*, 2016, **25**, 42–50.
54 D. Cai, D. Wang, B. Liu, L. Wang, Y. Liu, H. Li, Y. Wang, Q. Li and T. Wang, *ACS Appl. Mater. Interfaces*, 2016, **6**, 5050–5055.
55 M. Jing, H. Hou, C. E. Banks, Y. Yang, Y. Zhang and X. Ji, *ACS Appl. Mater. Interfaces*, 2015, **7**, 22741–22744.
56 X. Wang, S. Yao, X. Wu, Z. Shi, H. Sun and R. Que, *RSC Adv.*, 2015, **5**, 17938–17944.
57 L. Xie, F. Su, L. Xie, X. Li, Z. Liu, Q. Kong, X. Guo, Y. Zhang, L. Wan, K. Li, C. Lv and C. Chen, *ChemSusChem*, 2015, **8**, 2917–2926.